

العنوان:	Using finite element simulation to predict the effect of the preform cavity in two stage superplastic forming
المؤلف الرئيسي:	Jafar, Reem Ahmad Mousa
مؤلفين آخرين:	Al Huniti, Naser Shafei Najj(sup)
التاريخ الميلادي:	2014
موقع:	عمان
الصفحات:	1 - 105
رقم MD:	718234
نوع المحتوى:	رسائل جامعية
اللغة:	English
الدرجة العلمية:	رسالة ماجستير
الجامعة:	الجامعة الاردنية
الكلية:	كلية الدراسات العليا
الدولة:	الاردن
قواعد المعلومات:	Dissertations
مواضيع:	الهندسة الميكانيكية، التشكيل الفائق الطواعية
رابط:	<a href="https://search.mandumah.com/Record/718234">https://search.mandumah.com/Record/718234</a>

# USING FINITE ELEMENT SIMULATION TO PREDICT THE EFFECT OF THE PREFORM CAVITY IN TWO-STAGE SUPERPLASTIC FORMING

By  
**Reem Ahmad MousaJafar**

Supervisor  
**Dr. Naser S. Al-Huniti, Prof.**

## ABSTRACT

Superplastic Forming (SPF) is a high temperature forming operation for producing complex thin components in a single manufacturing process. It relies on the fact that certain materials can undergo large ductility under certain conditions. These conditions are forming within a specific range of strain rates, and forming in narrow ranges of temperature. The SPF process has many unique advantages over conventional forming operations including significant cost and weight savings potentials. However, the conventional SPF can result in excessive thinning at certain locations and produce a non-uniform thickness profile of the final formed part. To address these issues, a two-stage SPF process has been developed to improve the uniformity of thickness distribution. The two-stage SPF process is carried out by stretching the superplastic sheet at certain locations, while preserving material thickness in the regions experienced thinning in the conventional one-stage SPF, before the forward forming stage.

In this work, two techniques are applied to improve the final thickness distribution of a complex and practical shape, namely, the license plate pocket portion of the Oldsmobile Aurora decklid outer panel. These two techniques are the reverse free bulging and sheet preforming. The commercial finite element code, ABAQUS™, has been used to model the two-stage SPF process of an aluminum alloy AA5083 sheet at 450 °C. Finally, an engineered preform cavity has been designed to improve the thickness profile of the formed part.

It is found that the reverse free bulging technique did not result in the desired improvement in the thickness distribution of the final part. On the other hand, the two-stage SPF with sheet preforming has improved the thickness profile obtained from the one-stage SPF.

## استخدام محاكاة العنصر المحدود للتنبؤ بتأثير تجويف ما قبل التشكيل في التشكيل الفائق الطواعية ذو المرحلتين

إعداد

ريم أحمد موسى جعفر

المشرف

الأستاذ الدكتور ناصر الحنيطي

### ملخص

التشكيل الفائق الطواعية هي عملية تشكيل عند درجة حرارة عالية لإنتاج عناصر رقيقة معقدة في عملية تصنيع واحدة. تعتمد على حقيقة أن بعض المواد يمكن أن تخضع لليونة كبيرة في ظل ظروف معينة. هذه الظروف هي التشكيل ضمن نطاق محدد من معدلات الاجهاد، و التشكيل في نطاقات ضيقة لدرجة الحرارة. عملية التشكيل الفائق الطواعية لها العديد من المزايا الفريدة التي تميزها عن عمليات التشكيل التقليدية منها امكانيات كبيرة في توفير التكاليف و الوزن. لكن التشكيل الفائق الطواعية التقليدي يمكن أن يؤدي الى ترققات مفرطة في بعض المواقع و ينتج توزيع غير منتظم لسماكة الجزء النهائي المشكل. لمعالجة هذه القضايا، تم تطوير عملية تشكيل فائق الطواعية ذات مرحلتين لتحسين انتظام توزيع السمك. يتم تنفيذ العملية من خلال تمديد الصفيحة الفائقة الطواعية في مواقع معينة، مع الحفاظ على سمك المادة في المناطق التي شهدت ترقق في عملية التشكيل الفائق الطواعية التقليدية ذات المرحلة الواحدة، قبل مرحلة التشكيل الأمامية.

في هذا العمل، يتم تطبيق تقنيتين لتحسين توزيع السمك النهائي لشكل معقد و عملي، و هو، الجزء الخارجي من جيب لوحة رخصة سيارة. هاتان التقنيتان هما الانتفاخ الحر العكسي و التشكيل المسبق للصفيحة. البرنامج التجاري للعنصر المحدود، ABAQUS<sup>TM</sup> ، استخدم لتمثيل عملية التشكيل الفائق الطواعية ذات المرحلتين لصفيحة سبيكة الألمنيوم AA5083 عند درجة حرارة ٤٥٠ درجة مئوية. في النهاية، تم تصميم تجويف ما قبل التشكيل لتحسين توزيع سماكة الجزء الذي تم تشكيله.

وجد أن تقنية الانتفاخ الحر العكسي لم تؤدي الى التحسن المطلوب في توزيع سمك الجزء الأخير. من ناحية أخرى، التشكيل الفائق الطواعية ذو المرحلتين مع التشكيل المسبق للصفيحة حسن توزيع السمك الذي تم الحصول عليه من التشكيل الفائق الطواعية ذو المرحلة الواحدة.

العنوان:	Using finite element simulation to predict the effect of the preform cavity in two stage superplastic forming
المؤلف الرئيسي:	Jafar, Reem Ahmad Mousa
مؤلفين آخرين:	Al Huniti, Naser Shafei Najj(sup)
التاريخ الميلادي:	2014
موقع:	عمان
الصفحات:	1 - 105
رقم MD:	718234
نوع المحتوى:	رسائل جامعية
اللغة:	English
الدرجة العلمية:	رسالة ماجستير
الجامعة:	الجامعة الاردنية
الكلية:	كلية الدراسات العليا
الدولة:	الاردن
قواعد المعلومات:	Dissertations
مواضيع:	الهندسة الميكانيكية، التشكيل الفائق الطواعية
رابط:	<a href="https://search.mandumah.com/Record/718234">https://search.mandumah.com/Record/718234</a>

## LIST OF CONTENTS

Subject	Page
COMMITTEE DECISION .....	ii
DEDICATION.....	iii
ACKNOWLEDGMENTS .....	iv
LIST OF CONTENTS .....	v
LIST OF TABLES .....	viii
LIST OF FIGURES .....	ix
LIST OF ABBREVIATIONS AND SYMBOLS .....	xiii
ABSTRACT .....	xiv
<b>CHAPTER 1: INTRODUCTION</b> .....	<b>1</b>
1.1 Background .....	2
1.1.1 Superplasticity.....	2
1.1.2 History of Superplasticity .....	2
1.1.2.1 Before 1962 .....	3
1.1.2.2 From 1962 to 1982 .....	3
1.1.2.3 From 1982 to the Present .....	4
1.1.3 Superplastic Materials .....	4
1.1.3.1 Aluminum Alloys .....	5
1.1.3.2 Magnesium Alloys .....	5
1.1.3.3 Titanium Alloys .....	6
1.1.4 Material Behavior .....	6
1.1.5 Superplastic Forming Technique .....	9
1.1.6 Superplastic Forming Advantages .....	10
1.1.7 Superplastic Forming Limitations .....	11
1.1.8 Superplastic Forming Applications .....	12
1.2 Literature Survey .....	19
1.3 Motivation .....	22
1.4 Objectives .....	23
1.5 Research Methodology .....	24
1.6 Thesis Layout .....	26
<b>CHAPTER 2: MATERIAL MODEL DEVELOPMENT AND VERIFICATION</b> .....	<b>27</b>
2.1 Constitutive Model .....	28
2.1.1 Constitutive Model without Strain Hardening .....	28
2.1.2 Constitutive Model with Strain Hardening .....	30
2.2 Analytical Approach .....	33
2.2.1 Analytical Results for the Constitutive Model without	

Strain Hardening .....	35
2.2.2 Analytical Results for the Constitutive Model with Strain Hardening .....	37
2.3 Material Model Verification Using Finite Element Analysis.....	39
2.3.1 Creep Behavior in ABAQUS .....	41
2.3.2 ABAQUS Simulations .....	43
2.3.2.1 Constant Pressure Bulge Forming .....	44
2.3.2.2 Constant Strain Rate Bulge Forming .....	45
2.4 Results Comparison .....	47
2.5 Results Discussion and Material Model Summary .....	52
<b>CHAPTER 3: FINITE ELEMENT ANALYSIS OF ONE-STAGE SUPERPLASTIC FORMING PROCESS .....</b>	<b>54</b>
3.1 Introduction .....	54
3.2 Finite Element Analysis .....	56
3.2.1 Geometry and Model .....	56
3.2.2 Simulation Details .....	58
3.2.3 Mesh Convergence Study .....	59
3.3 Predicted Pressure and Thickness Profiles for the One-Stage SPF ..	64
<b>CHAPTER 4: FINITE ELEMENT ANALYSIS OF TWO-STAGE SUPERPLASTIC FORMING PROCESS .....</b>	<b>68</b>
4.1 Introduction .....	68
4.2 Reverse Free Bulging .....	68
4.2.1 Finite Element Analysis .....	70
4.2.1.1 Geometry and Model .....	70
4.2.1.2 Simulation Details .....	71
4.3 Two-Stage SPF (Sheet Preforming) .....	72
4.3.1 Finite Element Analysis .....	74
4.3.1.1 Preform Die Design .....	74
4.3.1.2 Geometry and Model .....	75
4.3.1.3 Simulation Details .....	78
<b>CHAPTER 5: RESULTS AND DISCUSSION .....</b>	<b>79</b>
5.1 Reverse Free Bulging .....	79
5.1.1 Predicted Gas Pressure Profile .....	80
5.1.2 Predicted Thickness Profile .....	81
5.2 Two-Stage SPF (Sheet Preforming) .....	83
5.2.1 Predicted Gas Pressure Profile .....	85
5.2.2 Predicted Thickness Profile .....	87
5.2.2.1 Thickness Profile at the End of the First Stage ...	87
5.2.2.2 Thickness Profile at the End of Forming .....	88
<b>CHAPTER 6: CONCLUSIONS AND RECOMMENDATIONS ....</b>	<b>93</b>

6.1 Conclusions .....	93
6.2 Future Work and Recommendations .....	95
REFERENCES .....	96
APPENDIX .....	101
Abstract (in Arabic).....	104

## LIST OF TABLES

NUMBER	TABLE CAPTION	PAGE
2.1	Upper yield point value of AA5083 for each strain rate.	30
2.2	The obtained m, n, and k values for each constitutive model.	33
2.3	The obtained m, n, and k values for others' models.	33
2.4	The material parameters A, n, and m for each constitutive model.	43
2.5	Forming time and minimum thickness for the two constant gas pressures.	45
2.6	Forming time and minimum thickness for the two constant gas strain rates.	46
2.7	Comparison between the analytical results and ABAQUS results for $\dot{\epsilon} = 0.001$ 1/sec.	52
2.8	Comparison between the analytical results and ABAQUS results for $\dot{\epsilon} = 0.0005$ 1/sec.	52
3.1	Mises equivalent stress results at MIDDLE_EL for different meshes.	61
3.2	Displacement in Y-direction results at MIDDLE_N for different meshes.	61
3.3	Percent difference between each two successive meshes for stress and displacement analysis.	63
5.1	Comparison in terms of forming time between the one-stage SPF and the two cases of reverse free bulging.	80
5.2	Comparison of the average and minimum thicknesses and thinning factor between the one-stage SPF and the two cases of reverse free bulging.	83
5.3	Comparison in terms of forming time between the one-stage SPF and the two-stage SPF using the four preform die models.	85
5.4	Comparison of the average and minimum thicknesses and thinning factor between the one-stage SPF and two-stage SPF.	90
5.5	Comparison of the cross-section length of line for the license plate pocket and that of the preform of model 4.	92



## LIST OF FIGURES

NUMBER	FIGURE CAPTION	PAGE
1.1	Comparison of conventional and superplastic tensile testing (Yarlagadda, et al., 2002).	2
1.2	Key discoveries in superplasticity in the early and middle part of the twentieth century (Nieh, et al., 1997).	3
1.3	Stress-strain rate curve for typical superplastic materials and the corresponding strain rate sensitivity (Abu-Farha, 2007).	8
1.4	Schematic illustration of a single-stage SPF die (Luckey, et al., 2009).	9
1.5	A schematic of the SPF technique (Abu-Farha, 2007).	10
1.6	Illustration of a typical thickness distribution for the SPF of a plane strain cross-section (Fischer, 1998).	11
1.7	Applications of SPF in the aerospace industry: (a) Rolls-Royce jet-engine fan blades (Grimes, 2005), (b) 737 Wing outboard leading edge strakelet (Hefti, 2007), (c) Location of the strakelet on the 737 wing leading edge (Hefti, 2007), and (d) Eurocopter air intake (Grimes, 2003).	14
1.8	Applications of SPF in the medical field: (a) A 2m diameter Siemens Magnet Technology (SMT) MRI scanner part ( <a href="http://www.superform-aluminum.com">www.superform-aluminum.com</a> ), (b) A titanium alloy ridge augmentation membrane (Curtis, 2005), (c) A nose reconstruction (Curtis, 2005), and (d) A dental prosthesis (Bonet, et al., 2006).	15
1.9	Applications of SPF in the automotive industry: (a) The modern Ford GT is clad with 10 superplastically formed body panels (Barnes, 2007), (b) A door panel (Bonet, et al., 2008), and (c) Aston Martin V12 Vanquish superformed body panels ( <a href="http://www.superform-aluminum.com">www.superform-aluminum.com</a> ).	16
1.10	Applications of SPF in the architectural field: (a) Tunnel cladding panels at Waterloo Station, London, UK, (b) Aluminum cladding panels at Grady Hospital, Atlanta Georgia, and (c) AA5083 curved panels at Victoria Island Shopping Mall, London, UK, ( <a href="http://www.superform-aluminum.com">www.superform-aluminum.com</a> ).	17
1.11	Applications of SPF in the train industry: (a) Two front panels of the Siemens Desiro UK train, and (b) Seat pans of the Heathrow Express fast rail link, ( <a href="http://www.superform-aluminum.com">www.superform-aluminum.com</a> ).	18
2.1	Tensile behavior of AA5083 at 450 °C for seven different strain rates (Krajewski and Montgomery, 2004).	29
2.2	Upper yield point of AA5083 for different strain rates at 450 °C.	30
2.3	Tensile test (Krajewski and Montgomery, 2004) and power curve fitting for $\dot{\epsilon} = 0.001$ 1/sec.	32
2.4	Tensile test (Krajewski and Montgomery, 2004) and power curve fitting for $\dot{\epsilon} = 0.0005$ 1/sec.	32
2.5	Schematic diagram of a bulged circular diaphragm (Jovane, 1968).	34

2.6	Analytical results for $\dot{\epsilon} = 0.001$ 1/sec (without strain hardening): (a) The relationship between the radius of curvature and time, (b) The variation in pole height with time, (c) The variation in pole thickness with time, and (d) The pressure-time curve.	36
2.7	Analytical results for $\dot{\epsilon} = 0.001$ 1/sec (with strain hardening): (a) The relationship between the radius of curvature and time, (b) The variation in pole height with time, (c) The variation in pole thickness with time, and (d) The pressure-time curve.	38
2.8	Analytical results for $\dot{\epsilon} = 0.0005$ 1/sec (with strain hardening): (a) The relationship between the radius of curvature and time, (b) The variation in pole height with time, (c) The variation in pole thickness with time, and (d) The pressure-time curve.	39
2.9	Finite element model used for simulating the SPF process.	40
2.10	The AA5083 sheet meshing.	40
2.11	Node ordering and face numbering on the 4-node element (ABAQUS™ Analysis User's Manual).	41
2.12	AA5083 bulge dome shape computed at 450 °C and a 0.29 MPa (42 psi) constant pressure.	45
2.13	AA5083 bulge dome shape computed at 450 °C and a 0.001 1/sec constant strain rate.	46
2.14	Dome pole height for AA5083 at 450 °C for FE models (solid lines) and GM experiment (triangles) (Bradley, 2004): (a) 0.29 MPa (42 psi), and (b) 0.56 MPa (81 psi).	48
2.15	Dome pole thickness for AA5083 at 450 °C for FE models (solid lines) and GM experiment (triangles) (Bradley, 2004): (a) 0.29 MPa (42 psi), and (b) 0.56 MPa (81 psi).	49
2.16	Dome pole height for AA5083 at 450 °C for FE models (solid lines) and analytical results (triangles): (a) $\dot{\epsilon} = 0.001$ 1/sec, and (b) $\dot{\epsilon} = 0.0005$ 1/sec.	50
2.17	Dome pole thickness for AA5083 at 450 °C for FE models (solid lines) and analytical results (triangles): (a) $\dot{\epsilon} = 0.001$ 1/sec, and (b) $\dot{\epsilon} = 0.0005$ 1/sec.	51
3.1	A superplastically formed license plate pocket (General Motors Corporation, Internal Report).	55
3.2	A 3D view of half of the license plate pocket die (General Motors Corporation, Internal Report).	55
3.3	The 2D model used for the simulation of the one-stage SPF.	56
3.4	A zoomed image for the AA5083 sheet modeled using 4 layers with 100 element per layer.	57
3.5	The die cross-section at the mid-section of the license plate pocket.	58
3.6	A zoomed image for the AA5083 sheet showing the location of the MIDDLE_EL (in red).	60

3.7	A zoomed image for the AA5083 sheet showing the location of the MIDDLE_N (in red).	60
3.8	Convergence results of the Mises equivalent stress (MPa) at MIDDLE_EL.	62
3.9	Convergence results of the displacement in Y-direction (mm) at MIDDLE_N.	62
3.10	The FE model used in the simulation at t = 21 seconds.	63
3.11	The deformed AA5083 sheet at different times during forming: (a) At t = 0 sec, (b) At t = 70.9 sec, (c) At t = 397.9 sec, and (d) At t = 900.9 sec.	65
3.12	The FE computed gas pressure profile for a target strain rate of 0.001 1/sec using the build-in ABAQUS algorithm.	66
3.13	The FE predicted thickness profile at the mid-section of the formed license plate pocket.	67
4.1	A schematic of the reverse free bulging process (Nazzal, et al., 2011).	69
4.2	The 2D model used for the simulation of the reverse free bulging.	71
4.3	The 2D models after the reverse free bulging stage: (a) Case 1 (first stage time = 40 seconds), and (b) Case 2 (first stage time = 80 seconds).	72
4.4	A schematic illustration of a two-stage SPF process (Luckey, et al., 2009).	73
4.5	The 2D models used for the simulation of two-stage SPF: (a) Model 1, (b) Model 2, (c) Model 3, and (d) Model 4.	76
4.6	The dimensions for each preform die design: (a) Model 1, (b) Model 2, (c) Model 3, and (d) Model 4.	77
5.1	The deformed AA5083 sheet for case 1 after: (a) the reverse free bulging stage (first stage), and (b) the forward forming stage (second stage).	79
5.2	The deformed AA5083 sheet for case 2 after: (a) the reverse free bulging stage (first stage), and (b) the forward forming stage (second stage).	80
5.3	The FE computed gas pressure profiles for a target strain rate of 0.001 1/sec for the two cases of reverse free bulging compared with that for the one-stage SPF.	81
5.4	The FE predicted thickness profiles at the mid-section of the formed license plate pocket for the two cases of reverse free bulging compared with that from the one-stage SPF.	82
5.5	The deformed AA5083 sheet for model 1 after: (a) the preforming stage, and (b) the forward forming stage.	84
5.6	The deformed AA5083 sheet for model 2 after: (a) the preforming stage, and (b) the forward forming stage.	84
5.7	The deformed AA5083 sheet for model 3 after: (a) the preforming stage, and (b) the forward forming stage.	84
5.8	The deformed AA5083 sheet for model 4 after: (a) the preforming stage, and (b) the forward forming stage.	85

5.9	The FE computed gas pressure profiles for the one-stage SPF and the four models used for the two-stage SPF.	86
5.10	The FE predicted thickness profiles after the preforming stage of the four models.	88
5.11	The FE predicted thickness profiles at the mid-section of the formed license plate pocket for the four models of the two-stage SPF compared with that from the one-stage SPF.	89
5.12	The FE predicted thickness profiles for the one-stage SPF and the two-stage SPF (model 4) compared with that after the preforming stage.	91
5.13	The FE predicted thickness profiles at the mid-section of the formed license plate pocket for the two-stage SPF (model 4) and that from the one-stage SPF.	92

## LIST OF ABBREVIATIONS AND SYMBOLS

SPF	Superplastic Forming
JIS	Japanese Industrial Standards
FEA	Finite element analysis
FE	Finite element
AA5083	Aluminum alloy 5083
MRI	Magnet resonance imaging
SMT	Siemens magnet technology
2D	Two-dimensional
3D	Three-dimensional
GM	General Motors
CPU	Central processing unit
$\sigma$	Effective flow stress (MPa)
$\varepsilon$	Effective strain
$\dot{\varepsilon}$	Effective strain rate (1/sec)
k	Strength coefficient
m	Strain rate sensitivity exponent
n	Strain hardening exponent
$\alpha_i$	Material parameters
$\rho$	Radius of curvature (mm)
a	Radius of the die (mm)
S	Thickness after some time (mm)
$S_0$	Original sheet thickness (mm)
t	Time (seconds)
P	Applied pressure (MPa)
h	Dome height (mm)
$\dot{\varepsilon}^{cr}$	Uniaxial equivalent creep strain rate (1/sec)
$\tilde{q}$	Uniaxial equivalent deviatoric stress (MPa)
$\bar{\varepsilon}^{cr}$	Equivalent creep strain
A, $\bar{m}$ and $\bar{n}$	Material parameters
$\dot{\varepsilon}_{max}$	Maximum equivalent creep strain rate (1/sec)
$\dot{\varepsilon}_{tar}$	Target creep strain rate (1/sec)
r	Strain rate ratio
$P_{new}$	New pressure magnitude (MPa)
$P_{old}$	Old pressure magnitude (MPa)
U2	Displacement in Y-direction (mm)
$L_{preform}$	Preform length of line (mm)
$L_{part}$	Part length of line (mm)

العنوان:	Using finite element simulation to predict the effect of the preform cavity in two stage superplastic forming
المؤلف الرئيسي:	Jafar, Reem Ahmad Mousa
مؤلفين آخرين:	Al Huniti, Naser Shafei Najj(sup)
التاريخ الميلادي:	2014
موقع:	عمان
الصفحات:	1 - 105
رقم MD:	718234
نوع المحتوى:	رسائل جامعية
اللغة:	English
الدرجة العلمية:	رسالة ماجستير
الجامعة:	الجامعة الاردنية
الكلية:	كلية الدراسات العليا
الدولة:	الاردن
قواعد المعلومات:	Dissertations
مواضيع:	الهندسة الميكانيكية، التشكيل الفائق الطواعية
رابط:	<a href="https://search.mandumah.com/Record/718234">https://search.mandumah.com/Record/718234</a>

**USING FINITE ELEMENT SIMULATION TO PREDICT THE  
EFFECT OF THE PREFORM CAVITY IN TWO-STAGE  
SUPERPLASTIC FORMING**

By

**Reem Ahmad Mousa Jafar**

Supervisor

**Dr. Naser S. Al-Huniti, Prof.**

**This Thesis was Submitted in Partial Fulfillment of the Requirements for the  
Master's Degree of Science in Mechanical Engineering**

**Faculty of Graduate Studies**

**The University of Jordan**

**May, 2014**

## نموذج ترخيص

أنا الطالبة: ريم أحمد موسى جعفر أمنح الجامعة الأردنية و /  
أو من تفوضه ترخيصاً غير حصري دون مقابل بنشر و / أو استعمال و / أو استغلال و /  
أو ترجمة و / أو تصوير و / أو إعادة إنتاج بأي طريقة كانت سواء ورقية و / أو إلكترونية  
أو غير ذلك رسالة الماجستير / الدكتوراه المقدمة من قبلي وعنوانها.

Using Finite Element Simulation to Predict the Effect  
of the Preform Cavity on Two-Stage Superplastic  
Forming.

وذلك لغايات البحث العلمي و / أو التبادل مع المؤسسات التعليمية والجامعات و / أو لأي  
غاية أخرى تراها الجامعة الأردنية مناسبة، وأمنح الجامعة الحق بالترخيص للغير بجميع أو  
بعض ما رخصته لها.

اسم الطالب: ريم أحمد موسى جعفر  
التوقيع: Reem Aljafar  
التاريخ: ٢٠١٤/٥/٢٠



## COMMITTEE DECISION

This Thesis (Using Finite Element Simulation to Predict the Effect of the Preform Cavity in Two-Stage Superplastic Forming) was Successfully Defended and Approved on May 14, 2014

### Examination Committee

### Signature

Dr. Naser Al-Huniti (Supervisor)  
Prof. of Applied Mechanics

*Naser Al-Huniti*

Dr. Osama Abu Zeid (Member)  
Prof. of Applied Mechanics

*Osama Abu Zeid*

Dr. Moudar Zgoul (Member)  
Assoc. Prof. of Applied Mechanics

*M. Zgoul*

Dr. Saad Al-Hubaili (Member/ External Examiner)  
Prof. of Applied Mechanics  
(Retired)

*Saad Al-Hubaili*

تعتمد كلية الدراسات العليا  
هذه النسخة من الرسالة  
الترقيم.....التاريخ.....

*Dr. Saad Al-Hubaili*

## DEDICATION

Dedicated To My Parents, Husband and Sisters

## ACKNOWLEDGEMENT

I would like to express my sincere gratitude to my supervisor Prof. Naser Al-Huniti for his support, patience, and motivation. His guidance helped me in all the time of research and writing this thesis.

I am also deeply thankful to Dr. Firas Jarrar for his continuous support. I was motivated by his knowledge in superplastic forming. Thank you for believing in my abilities and helping me in all stages of this thesis.

Last but not least, I would like to thank my parents, husband and sisters for always believing in me, for their continuous love and their support. This thesis would not have been possible without your help.

## LIST OF CONTENTS

Subject	Page
COMMITTEE DECISION .....	ii
DEDICATION.....	iii
ACKNOWLEDGMENTS .....	iv
LIST OF CONTENTS .....	v
LIST OF TABLES .....	viii
LIST OF FIGURES .....	ix
LIST OF ABBREVIATIONS AND SYMBOLS .....	xiii
ABSTRACT .....	xiv
<b>CHAPTER 1: INTRODUCTION</b> .....	<b>1</b>
1.1 Background .....	2
1.1.1 Superplasticity.....	2
1.1.2 History of Superplasticity .....	2
1.1.2.1 Before 1962 .....	3
1.1.2.2 From 1962 to 1982 .....	3
1.1.2.3 From 1982 to the Present .....	4
1.1.3 Superplastic Materials .....	4
1.1.3.1 Aluminum Alloys .....	5
1.1.3.2 Magnesium Alloys .....	5
1.1.3.3 Titanium Alloys .....	6
1.1.4 Material Behavior .....	6
1.1.5 Superplastic Forming Technique .....	9
1.1.6 Superplastic Forming Advantages .....	10
1.1.7 Superplastic Forming Limitations .....	11
1.1.8 Superplastic Forming Applications .....	12
1.2 Literature Survey .....	19
1.3 Motivation .....	22
1.4 Objectives .....	23
1.5 Research Methodology .....	24
1.6 Thesis Layout .....	26
<b>CHAPTER 2: MATERIAL MODEL DEVELOPMENT AND VERIFICATION</b> .....	<b>27</b>
2.1 Constitutive Model .....	28
2.1.1 Constitutive Model without Strain Hardening .....	28
2.1.2 Constitutive Model with Strain Hardening .....	30
2.2 Analytical Approach .....	33
2.2.1 Analytical Results for the Constitutive Model without	

Strain Hardening .....	35
2.2.2 Analytical Results for the Constitutive Model with Strain Hardening .....	37
2.3 Material Model Verification Using Finite Element Analysis.....	39
2.3.1 Creep Behavior in ABAQUS .....	41
2.3.2 ABAQUS Simulations .....	43
2.3.2.1 Constant Pressure Bulge Forming .....	44
2.3.2.2 Constant Strain Rate Bulge Forming .....	45
2.4 Results Comparison .....	47
2.5 Results Discussion and Material Model Summary .....	52
<b>CHAPTER 3: FINITE ELEMENT ANALYSIS OF ONE-STAGE SUPERPLASTIC FORMING PROCESS .....</b>	<b>54</b>
3.1 Introduction .....	54
3.2 Finite Element Analysis .....	56
3.2.1 Geometry and Model .....	56
3.2.2 Simulation Details .....	58
3.2.3 Mesh Convergence Study .....	59
3.3 Predicted Pressure and Thickness Profiles for the One-Stage SPF ..	64
<b>CHAPTER 4: FINITE ELEMENT ANALYSIS OF TWO-STAGE SUPERPLASTIC FORMING PROCESS .....</b>	<b>68</b>
4.1 Introduction .....	68
4.2 Reverse Free Bulging .....	68
4.2.1 Finite Element Analysis .....	70
4.2.1.1 Geometry and Model .....	70
4.2.1.2 Simulation Details .....	71
4.3 Two-Stage SPF (Sheet Preforming) .....	72
4.3.1 Finite Element Analysis .....	74
4.3.1.1 Preform Die Design .....	74
4.3.1.2 Geometry and Model .....	75
4.3.1.3 Simulation Details .....	78
<b>CHAPTER 5: RESULTS AND DISCUSSION .....</b>	<b>79</b>
5.1 Reverse Free Bulging .....	79
5.1.1 Predicted Gas Pressure Profile .....	80
5.1.2 Predicted Thickness Profile .....	81
5.2 Two-Stage SPF (Sheet Preforming) .....	83
5.2.1 Predicted Gas Pressure Profile .....	85
5.2.2 Predicted Thickness Profile .....	87
5.2.2.1 Thickness Profile at the End of the First Stage ...	87
5.2.2.2 Thickness Profile at the End of Forming .....	88
<b>CHAPTER 6: CONCLUSIONS AND RECOMMENDATIONS ....</b>	<b>93</b>

6.1 Conclusions .....	93
6.2 Future Work and Recommendations .....	95
REFERENCES .....	96
APPENDIX .....	101
Abstract (in Arabic).....	104

## LIST OF TABLES

NUMBER	TABLE CAPTION	PAGE
2.1	Upper yield point value of AA5083 for each strain rate.	30
2.2	The obtained m, n, and k values for each constitutive model.	33
2.3	The obtained m, n, and k values for others' models.	33
2.4	The material parameters A, n, and m for each constitutive model.	43
2.5	Forming time and minimum thickness for the two constant gas pressures.	45
2.6	Forming time and minimum thickness for the two constant gas strain rates.	46
2.7	Comparison between the analytical results and ABAQUS results for $\dot{\epsilon} = 0.001$ 1/sec.	52
2.8	Comparison between the analytical results and ABAQUS results for $\dot{\epsilon} = 0.0005$ 1/sec.	52
3.1	Mises equivalent stress results at MIDDLE_EL for different meshes.	61
3.2	Displacement in Y-direction results at MIDDLE_N for different meshes.	61
3.3	Percent difference between each two successive meshes for stress and displacement analysis.	63
5.1	Comparison in terms of forming time between the one-stage SPF and the two cases of reverse free bulging.	80
5.2	Comparison of the average and minimum thicknesses and thinning factor between the one-stage SPF and the two cases of reverse free bulging.	83
5.3	Comparison in terms of forming time between the one-stage SPF and the two-stage SPF using the four preform die models.	85
5.4	Comparison of the average and minimum thicknesses and thinning factor between the one-stage SPF and two-stage SPF.	90
5.5	Comparison of the cross-section length of line for the license plate pocket and that of the preform of model 4.	92

## LIST OF FIGURES

NUMBER	FIGURE CAPTION	PAGE
1.1	Comparison of conventional and superplastic tensile testing (Yarlagadda, et al., 2002).	2
1.2	Key discoveries in superplasticity in the early and middle part of the twentieth century (Nieh, et al., 1997).	3
1.3	Stress-strain rate curve for typical superplastic materials and the corresponding strain rate sensitivity (Abu-Farha, 2007).	8
1.4	Schematic illustration of a single-stage SPF die (Luckey, et al., 2009).	9
1.5	A schematic of the SPF technique (Abu-Farha, 2007).	10
1.6	Illustration of a typical thickness distribution for the SPF of a plane strain cross-section (Fischer, 1998).	11
1.7	Applications of SPF in the aerospace industry: (a) Rolls-Royce jet-engine fan blades (Grimes, 2005), (b) 737 Wing outboard leading edge strakelet (Hefti, 2007), (c) Location of the strakelet on the 737 wing leading edge (Hefti, 2007), and (d) Eurocopter air intake (Grimes, 2003).	14
1.8	Applications of SPF in the medical field: (a) A 2m diameter Siemens Magnet Technology (SMT) MRI scanner part ( <a href="http://www.superform-aluminum.com">www.superform-aluminum.com</a> ), (b) A titanium alloy ridge augmentation membrane (Curtis, 2005), (c) A nose reconstruction (Curtis, 2005), and (d) A dental prosthesis (Bonet, et al., 2006).	15
1.9	Applications of SPF in the automotive industry: (a) The modern Ford GT is clad with 10 superplastically formed body panels (Barnes, 2007), (b) A door panel (Bonet, et al., 2008), and (c) Aston Martin V12 Vanquish superformed body panels ( <a href="http://www.superform-aluminum.com">www.superform-aluminum.com</a> ).	16
1.10	Applications of SPF in the architectural field: (a) Tunnel cladding panels at Waterloo Station, London, UK, (b) Aluminum cladding panels at Grady Hospital, Atlanta Georgia, and (c) AA5083 curved panels at Victoria Island Shopping Mall, London, UK, ( <a href="http://www.superform-aluminum.com">www.superform-aluminum.com</a> ).	17
1.11	Applications of SPF in the train industry: (a) Two front panels of the Siemens Desiro UK train, and (b) Seat pans of the Heathrow Express fast rail link, ( <a href="http://www.superform-aluminum.com">www.superform-aluminum.com</a> ).	18
2.1	Tensile behavior of AA5083 at 450 °C for seven different strain rates (Krajewski and Montgomery, 2004).	29
2.2	Upper yield point of AA5083 for different strain rates at 450 °C.	30
2.3	Tensile test (Krajewski and Montgomery, 2004) and power curve fitting for $\dot{\epsilon} = 0.001$ 1/sec.	32
2.4	Tensile test (Krajewski and Montgomery, 2004) and power curve fitting for $\dot{\epsilon} = 0.0005$ 1/sec.	32
2.5	Schematic diagram of a bulged circular diaphragm (Jovane, 1968).	34



2.6	Analytical results for $\dot{\epsilon} = 0.001$ 1/sec (without strain hardening): (a) The relationship between the radius of curvature and time, (b) The variation in pole height with time, (c) The variation in pole thickness with time, and (d) The pressure-time curve.	36
2.7	Analytical results for $\dot{\epsilon} = 0.001$ 1/sec (with strain hardening): (a) The relationship between the radius of curvature and time, (b) The variation in pole height with time, (c) The variation in pole thickness with time, and (d) The pressure-time curve.	38
2.8	Analytical results for $\dot{\epsilon} = 0.0005$ 1/sec (with strain hardening): (a) The relationship between the radius of curvature and time, (b) The variation in pole height with time, (c) The variation in pole thickness with time, and (d) The pressure-time curve.	39
2.9	Finite element model used for simulating the SPF process.	40
2.10	The AA5083 sheet meshing.	40
2.11	Node ordering and face numbering on the 4-node element (ABAQUS™ Analysis User's Manual).	41
2.12	AA5083 bulge dome shape computed at 450 °C and a 0.29 MPa (42 psi) constant pressure.	45
2.13	AA5083 bulge dome shape computed at 450 °C and a 0.001 1/sec constant strain rate.	46
2.14	Dome pole height for AA5083 at 450 °C for FE models (solid lines) and GM experiment (triangles) (Bradley, 2004): (a) 0.29 MPa (42 psi), and (b) 0.56 MPa (81 psi).	48
2.15	Dome pole thickness for AA5083 at 450 °C for FE models (solid lines) and GM experiment (triangles) (Bradley, 2004): (a) 0.29 MPa (42 psi), and (b) 0.56 MPa (81 psi).	49
2.16	Dome pole height for AA5083 at 450 °C for FE models (solid lines) and analytical results (triangles): (a) $\dot{\epsilon} = 0.001$ 1/sec, and (b) $\dot{\epsilon} = 0.0005$ 1/sec.	50
2.17	Dome pole thickness for AA5083 at 450 °C for FE models (solid lines) and analytical results (triangles): (a) $\dot{\epsilon} = 0.001$ 1/sec, and (b) $\dot{\epsilon} = 0.0005$ 1/sec.	51
3.1	A superplastically formed license plate pocket (General Motors Corporation, Internal Report).	55
3.2	A 3D view of half of the license plate pocket die (General Motors Corporation, Internal Report).	55
3.3	The 2D model used for the simulation of the one-stage SPF.	56
3.4	A zoomed image for the AA5083 sheet modeled using 4 layers with 100 element per layer.	57
3.5	The die cross-section at the mid-section of the license plate pocket.	58
3.6	A zoomed image for the AA5083 sheet showing the location of the MIDDLE_EL (in red).	60

3.7	A zoomed image for the AA5083 sheet showing the location of the MIDDLE_N (in red).	60
3.8	Convergence results of the Mises equivalent stress (MPa) at MIDDLE_EL.	62
3.9	Convergence results of the displacement in Y-direction (mm) at MIDDLE_N.	62
3.10	The FE model used in the simulation at $t = 21$ seconds.	63
3.11	The deformed AA5083 sheet at different times during forming: (a) At $t = 0$ sec, (b) At $t = 70.9$ sec, (c) At $t = 397.9$ sec, and (d) At $t = 900.9$ sec.	65
3.12	The FE computed gas pressure profile for a target strain rate of 0.001 1/sec using the build-in ABAQUS algorithm.	66
3.13	The FE predicted thickness profile at the mid-section of the formed license plate pocket.	67
4.1	A schematic of the reverse free bulging process (Nazzal, et al., 2011).	69
4.2	The 2D model used for the simulation of the reverse free bulging.	71
4.3	The 2D models after the reverse free bulging stage: (a) Case 1 (first stage time = 40 seconds), and (b) Case 2 (first stage time = 80 seconds).	72
4.4	A schematic illustration of a two-stage SPF process (Luckey, et al., 2009).	73
4.5	The 2D models used for the simulation of two-stage SPF: (a) Model 1, (b) Model 2, (c) Model 3, and (d) Model 4.	76
4.6	The dimensions for each preform die design: (a) Model 1, (b) Model 2, (c) Model 3, and (d) Model 4.	77
5.1	The deformed AA5083 sheet for case 1 after: (a) the reverse free bulging stage (first stage), and (b) the forward forming stage (second stage).	79
5.2	The deformed AA5083 sheet for case 2 after: (a) the reverse free bulging stage (first stage), and (b) the forward forming stage (second stage).	80
5.3	The FE computed gas pressure profiles for a target strain rate of 0.001 1/sec for the two cases of reverse free bulging compared with that for the one-stage SPF.	81
5.4	The FE predicted thickness profiles at the mid-section of the formed license plate pocket for the two cases of reverse free bulging compared with that from the one-stage SPF.	82
5.5	The deformed AA5083 sheet for model 1 after: (a) the preforming stage, and (b) the forward forming stage.	84
5.6	The deformed AA5083 sheet for model 2 after: (a) the preforming stage, and (b) the forward forming stage.	84
5.7	The deformed AA5083 sheet for model 3 after: (a) the preforming stage, and (b) the forward forming stage.	84
5.8	The deformed AA5083 sheet for model 4 after: (a) the preforming stage, and (b) the forward forming stage.	85

5.9	The FE computed gas pressure profiles for the one-stage SPF and the four models used for the two-stage SPF.	86
5.10	The FE predicted thickness profiles after the preforming stage of the four models.	88
5.11	The FE predicted thickness profiles at the mid-section of the formed license plate pocket for the four models of the two-stage SPF compared with that from the one-stage SPF.	89
5.12	The FE predicted thickness profiles for the one-stage SPF and the two-stage SPF (model 4) compared with that after the preforming stage.	91
5.13	The FE predicted thickness profiles at the mid-section of the formed license plate pocket for the two-stage SPF (model 4) and that from the one-stage SPF.	92

## LIST OF ABBREVIATIONS AND SYMBOLS

SPF	Superplastic Forming
JIS	Japanese Industrial Standards
FEA	Finite element analysis
FE	Finite element
AA5083	Aluminum alloy 5083
MRI	Magnet resonance imaging
SMT	Siemens magnet technology
2D	Two-dimensional
3D	Three-dimensional
GM	General Motors
CPU	Central processing unit
$\sigma$	Effective flow stress (MPa)
$\varepsilon$	Effective strain
$\dot{\varepsilon}$	Effective strain rate (1/sec)
k	Strength coefficient
m	Strain rate sensitivity exponent
n	Strain hardening exponent
$\alpha_i$	Material parameters
$\rho$	Radius of curvature (mm)
a	Radius of the die (mm)
S	Thickness after some time (mm)
$S_0$	Original sheet thickness (mm)
t	Time (seconds)
P	Applied pressure (MPa)
h	Dome height (mm)
$\dot{\varepsilon}^{cr}$	Uniaxial equivalent creep strain rate (1/sec)
$\tilde{q}$	Uniaxial equivalent deviatoric stress (MPa)
$\bar{\varepsilon}^{cr}$	Equivalent creep strain
A, $\bar{m}$ and $\bar{n}$	Material parameters
$\dot{\varepsilon}_{max}$	Maximum equivalent creep strain rate (1/sec)
$\dot{\varepsilon}_{tar}$	Target creep strain rate (1/sec)
r	Strain rate ratio
$P_{new}$	New pressure magnitude (MPa)
$P_{old}$	Old pressure magnitude (MPa)
U2	Displacement in Y-direction (mm)
$L_{preform}$	Preform length of line (mm)
$L_{part}$	Part length of line (mm)

# USING FINITE ELEMENT SIMULATION TO PREDICT THE EFFECT OF THE PREFORM CAVITY IN TWO-STAGE SUPERPLASTIC FORMING

By  
**Reem Ahmad MousaJafar**

Supervisor  
**Dr. Naser S. Al-Huniti, Prof.**

## ABSTRACT

Superplastic Forming (SPF) is a high temperature forming operation for producing complex thin components in a single manufacturing process. It relies on the fact that certain materials can undergo large ductility under certain conditions. These conditions are forming within a specific range of strain rates, and forming in narrow ranges of temperature. The SPF process has many unique advantages over conventional forming operations including significant cost and weight savings potentials. However, the conventional SPF can result in excessive thinning at certain locations and produce a non-uniform thickness profile of the final formed part. To address these issues, a two-stage SPF process has been developed to improve the uniformity of thickness distribution. The two-stage SPF process is carried out by stretching the superplastic sheet at certain locations, while preserving material thickness in the regions experienced thinning in the conventional one-stage SPF, before the forward forming stage.

In this work, two techniques are applied to improve the final thickness distribution of a complex and practical shape, namely, the license plate pocket portion of the Oldsmobile Aurora decklid outer panel. These two techniques are the reverse free bulging and sheet preforming. The commercial finite element code, ABAQUS™, has been used to model the two-stage SPF process of an aluminum alloy AA5083 sheet at 450 °C. Finally, an engineered preform cavity has been designed to improve the thickness profile of the formed part.

It is found that the reverse free bulging technique did not result in the desired improvement in the thickness distribution of the final part. On the other hand, the two-stage SPF with sheet preforming has improved the thickness profile obtained from the one-stage SPF.

## CHAPTER 1

### INTRODUCTION

Superplastic forming (SPF) is a high temperature forming operation for producing complex thin sheet components in a single manufacturing process. It relies on the fact that some materials can undergo large ductility under certain conditions.

The SPF has many unique advantages over conventional forming processes including greater design flexibility, forming light weight components with complex geometries in one manufacturing step, low dies cost and the elimination of spring back. Although SPF offers many advantages it still faces many problems that hamper its widespread use. These limitations include the non-uniformity of the produced part thickness, long forming times, the possibility of severe thinning and necking at certain locations and large amounts of cavities developed in some superplastic alloys.

Two-stage SPF is a process that utilizes two stages of gas forming within one die. During the first stage, the superplastic material sheet is forced to take the shape of the preform cavity. This preform cavity is designed in a way to pre-stretch the sheet and increase the thickness at the critical locations which experienced thinning in the conventional SPF. Currently, the two-stage SPF process is mainly based on finite element analysis (FEA) and experimental iterations.

In order for the two-stage SPF process to become an efficient forming operation, its output should be predictable and the forming time must be reduced without compromising the integrity of the produced parts. In addition, the thickness distribution of the formed

parts must be improved, even though a certain amount of deviation cannot be avoided due to the stretching of the sheet. All of this requires developing accurate material models and the execution of thorough experimental and numerical investigations.

## 1.1 Background

### 1.1.1 Superplasticity

Superplasticity is the ability of certain type of materials to exhibit large tensile deformation prior to fracture. The conditions for superplasticity to occur are forming within a specific range of strain rates, and forming in narrow ranges of temperatures. Each material has a unique optimum value of strain rate, and a narrow temperature range which lies above half the material's absolute melting point (Lin, 2003). Figure 1.1 shows a comparison between conventional and superplastic tensile testing of an Aluminum specimen (Yarlagadda, et al., 2002).



Figure 1.1 Comparison of conventional and superplastic tensile testing (Yarlagadda, et al., 2002).

### 1.1.2 History of Superplasticity

The history of superplasticity can be divided into three main time periods: before 1962, from 1962 to 1982, and from 1982 to the present.

### 1.1.2.1 Before 1962

According to Nieh, et al. (1997) this stage began with a paper published by Bengoughin 1912 which is believed to contain the first recorded description of superplasticity in a metallic material. In 1934, Pearson observed the unusual large elongations that could be achieved in certain fine-structured materials. Later on, in 1945, Bochvar and Sviderskajo put the expression Superplastichnost (ultrahigh plasticity) in their paper on superplastic alloys. The term Superplasticity first appeared in a technical paper by Lozinsky and Simeonovain 1959. Figure 1.2 summarizes the key observations and discoveries in superplasticity through this stage (Nieh, et al., 1997).

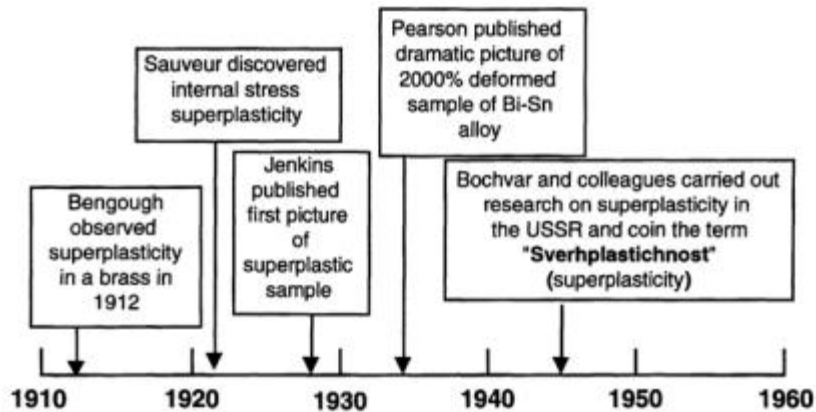


Figure 1.2 Key discoveries in superplasticity in the early and middle part of the twentieth century (Nieh, et al., 1997).

### 1.1.2.2 From 1962 to 1982

The major increase in interest in superplasticity came in 1964, when Backofen, et al. published a paper suggesting applying polymer and glass forming techniques in superplastic metals forming. By 1969, the first book entitled *Superplasticity of Metals and Alloys* was published by Presnyakov. After that, numerous papers on superplasticity were



issued. Following these publications, SPF became a process for manufacturing lightweight complex components in many applications.

### **1.1.2.3 From 1982 to the Present**

During this time period, many conferences were held on SPF, and numerous papers were published to eliminate the limitations of SPF that hamper its widespread use. In the present stage, the focus is pointed towards making SPF the manufacturing choice for lightweight complex components in high rate mass production.

### **1.1.3 Superplastic Materials**

Superplastic materials are polycrystalline solids which, under certain conditions, have the capability to exhibit very large elongations, i.e. >500%. While the maximum elongation prior to failure that can be achieved in conventional alloys does not exceed 120%, regardless of the pulling speed or temperature (Pilling and Ridley, 1989). However, large elongations usually occur in a low strain rate range from  $10^{-5}$  to  $10^{-3}$   $s^{-1}$ . Superplasticity which occur at strain rates  $>10^{-2}$   $s^{-1}$  is defined as high strain rate superplasticity in Japanese Industrial Standards (JIS) H 7007 by Japanese Standards Association. Aluminum- and titanium-based materials are high strain rate superplastic materials (Yarlagadda, et al., 2002).

Superplasticity has been noticed in various types of materials, such as ceramics (including composites and monoliths), metals (including aluminum, iron, magnesium, titanium and nickel-based alloys), intermetallics (including iron, nickel, and titanium base)

and laminates (Xing, et al., 2004). The main metallurgical requirements for these materials to exhibit superplasticity are fine equi-axed grain structure, grain size in the range of 2 to 10 micrometers (Pilling and Ridley, 1989), and a resistance to both grain growth and cavities formation (Siegert and Werle, 1994).

### **1.1.3.1 Aluminum Alloys**

Aluminum alloys have been used to produce superplastically formed parts for the automotive, aerospace, marine, and architectural industries (Osada, 1997, Nakamura, et al. 1997 and Barnes, 1999). These alloys can be used where low weight and high stiffness are required (Xing, et al., 2004). The main characteristics of Aluminum alloys are: low weight, good corrosion resistance, and relatively moderate strength (Verma, et al., 1996). Superplastically formed Aluminum alloys have the ability to be stretched to several times their original size without failure when heated to between 470 – 520 °C (Mikhailovskaya, et al., 2012).

### **1.1.3.2 Magnesium Alloys**

Magnesium has been receiving a great attention over the last decade since it is the lightest constructional metal on earth (Nazzal, et al., 2011, a). Magnesium alloys are attractive for applications where light weight and rigidity are the key elements for component design. The lower density of Magnesium over currently used aerospace Aluminum alloys have been the dominant driving force for using Magnesium alloys. However, these alloys have relatively low strength which restricts their usage to

applications where high strength is not necessarily needed (Park, et al., 1996 and Carrino, et al., 2013).

### 1.1.3.3 Titanium Alloys

Titanium alloys have been used in aerospace and automobile industries. The main characteristics of these alloys are: low weight-size ratio, high relative strength, resistance to corrosion, high temperature creep resistance, and they do not need post-forming heat treatment (Sieniawski and Motyka, 2007 and Yarlalagadda, et al., 2002). Titanium alloy Ti-6Al-4V has both excellent biocompatibility and superior mechanical properties. It can be deformed greatly and easily at the superplastic temperature range of 800 - 900 °C (Okuno, et al., 1989).

### 1.1.4 Material Behavior

Materials undergoing the superplastic forming operation have common characteristics including a fine and stable grain size, and a low flow stress. The flow stress in these materials is highly sensitive to the strain rate. A simple form of the constitutive equation that describes this strain rate dependence for superplastic materials is given by (Avery and Backofen, 1965):

$$\sigma = k\dot{\epsilon}^m \quad (1.1)$$

Where  $\sigma$  is the effective flow stress,  $\dot{\epsilon}$  is the effective strain rate,  $k$  is the strength coefficient, and  $m$  is the strain rate sensitivity exponent, which should be greater than 0.3

for superplastic behavior to exist (Pilling and Ridley, 1989). The strain rate sensitivity exponent or the  $m$ -value, which ranges from 0.3 to 0.8 for superplastic materials, is a measure of a material's ability to resist necking. Higher values of  $m$  gives higher tensile elongation behavior for superplastic materials (Avery and Backofen, 1965).

The function of strain rate sensitivity in necking resistance can be explained by considering tensile testing of a specimen under a constant strain rate condition. When a neck begins to develop, the strain rate locally increases in the necked region and becomes larger than the strain rate in the rest of the tensile specimen. According to equation (1.1) and because of the high value of  $m$ , the desired flow stress would increase sharply in response to the increase in the strain rate in the necked region in order to continue deformation in that region. This would cause the material flow to occur outside the necked region. Thus, strain rate hardening in that region prevents additional necking development (Pilling and Ridley, 1989 and Siegert and Werle, 1994). As a result, a high  $m$ -value gives a high resistance to neck development and leads to high tensile elongations prior to failure characteristic of superplastic materials (Hedworth and Stowel, 1971).

A typical stress/strain rate relation for superplastic materials is shown on logarithmic scales in figure 1.3. According to equation 1.1, the slope of the curve is equal to the strain rate sensitivity exponent; this can also be seen from the second part of figure 1.3, which shows the variation of the strain rate sensitivity exponent with strain rate. The sigmoidal shape in figure 1.3 can be divided into three regions based on the  $m$ -value. Note that regions I and III, which represent the low strain rate and high strain rate regions, respectively, have a strain rate sensitivity exponent value of less than 0.3. Thus, superplasticity is not observed when forming under the conditions of these two regions. On

the other hand, superplasticity occurs only in region II, which is the moderate strain rate region, where the strain rate sensitivity exponent has values greater than 0.3, accompanied by very large elongations. Unfortunately, this moderate strain rate region ranges between  $10^{-5} - 10^{-2}$  1/sec, which is considered very low for high production rates.

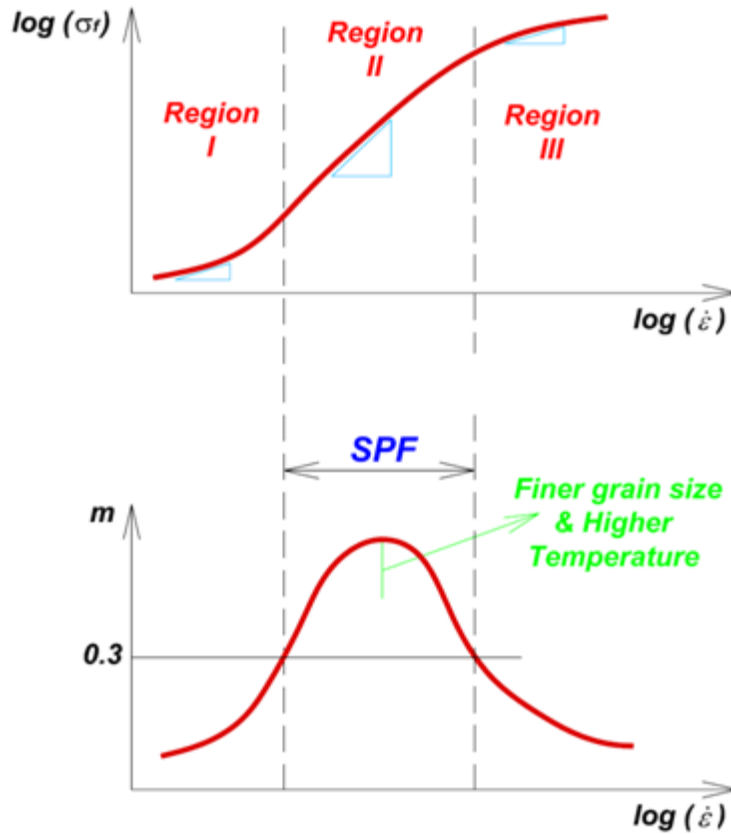


Figure 1.3 Stress-strain rate curve for typical superplastic materials and the corresponding strain rate sensitivity (Abu-Farha, 2007).

It should be noted here that the mechanical behavior of superplastic materials is very sensitive to both temperature and grain size. Generally, increasing the forming temperature or decreasing the grain size of the material increases both the strain rate sensitivity exponent and the strain rate, however the flow stresses decrease (Pilling and

Ridley, 1989).

### 1.1.5 Superplastic Forming Technique

The SPF process is carried out by heating a sheet of superplastic material placed on a single-sided die. As mentioned previously, the sheet is heated to the required SPF temperature which is specified for that material. Then, an inert gas is applied to one side of the sheet to control the rate of deformation and force the sheet to take the shape of the die cavity. The SPF process is illustrated schematically in figure 1.4.

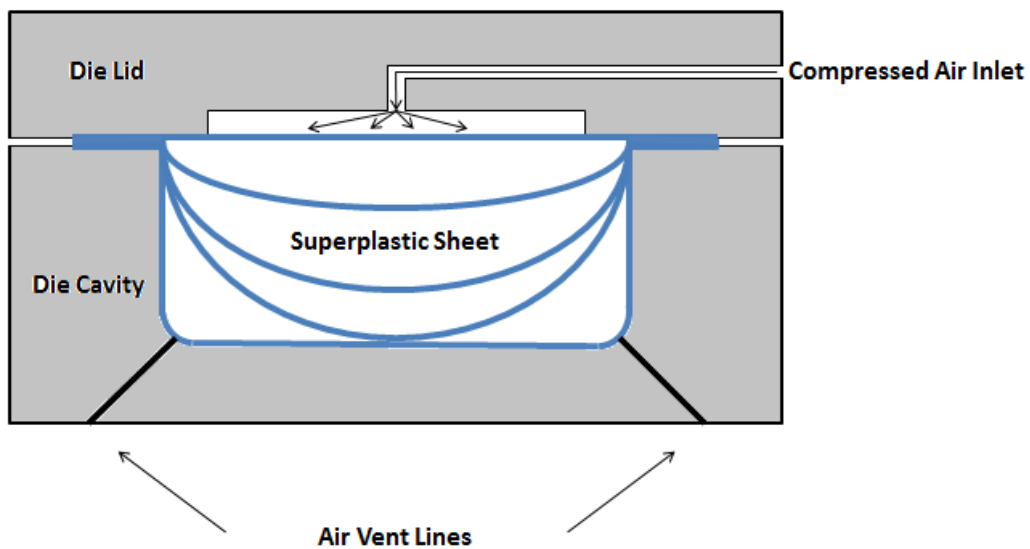


Figure 1.4 Schematic illustration of a single-stage SPF die (Luckey, et al., 2009).

There are two main types of SPF, cavity forming and bubble forming. Cavity forming is most commonly used and ideal for producing large complex parts such as car body panels, building cladding panels and large rail parts. This process is ideally suited to forming 5083 aluminum alloys and Magnesium. In cavity forming a sheet of superplastic material is heated and placed on a single-sided die. A pressurized gas is then applied to one side of the sheet forcing it to take the shape of the die cavity. The other type of SPF, which is referred to as bubble forming, is ideal for producing small components, where material

العنوان:	Using finite element simulation to predict the effect of the preform cavity in two stage superplastic forming
المؤلف الرئيسي:	Jafar, Reem Ahmad Mousa
مؤلفين آخرين:	Al Huniti, Naser Shafei Najj(sup)
التاريخ الميلادي:	2014
موقع:	عمان
الصفحات:	1 - 105
رقم MD:	718234
نوع المحتوى:	رسائل جامعية
اللغة:	English
الدرجة العلمية:	رسالة ماجستير
الجامعة:	الجامعة الاردنية
الكلية:	كلية الدراسات العليا
الدولة:	الاردن
قواعد المعلومات:	Dissertations
مواضيع:	الهندسة الميكانيكية، التشكيل الفائق الطواعية
رابط:	<a href="https://search.mandumah.com/Record/718234">https://search.mandumah.com/Record/718234</a>

**USING FINITE ELEMENT SIMULATION TO PREDICT THE  
EFFECT OF THE PREFORM CAVITY IN TWO-STAGE  
SUPERPLASTIC FORMING**

By

**Reem Ahmad Mousa Jafar**

Supervisor

**Dr. Naser S. Al-Huniti, Prof.**

**This Thesis was Submitted in Partial Fulfillment of the Requirements for the  
Master's Degree of Science in Mechanical Engineering**

**Faculty of Graduate Studies**

**The University of Jordan**

**May, 2014**